National Laboratory Field Work
Annual Progress Report

Project Title: Crosscutting Applications for a New Class of Ultra-Hard Materials Based on $AlMgB_{14}$

Covering Period: October 1, 2002 to September 30, 2003

Date of Report: December 1, 2003

Laboratory: Ames Laboratory, Materials and Engineering Physics Program
Iowa State University, Ames, IA 50011-3020

FWP/OTIS Number: AL-01-501-043

Contact: Dr. Bruce Cook (515-294-9673, cook@ameslab.gov)
Prof. Alan Russell (515-294-3204, russell@iastate.edu)

Table of Contents

Subcontractor

University of Arkansas, Department of Mechanical Engineering, Fayetteville, AR

Research Partners

Praxair Surface Technologies, Indianapolis, IN
Deere & Co. Technical Center, Moline, IL
Michigan Technical University, Houghton, MI
Boise Cascade Corp., Wallula, WA
Brunner & Lay Inc, Springdale, AR
Kennametal, Latrobe, PA

Project Team

Dr. Sara Dillich (DOE-HQ)
Dr. Tom Taylor, Praxair Surface Technologies
Dr. Bruce Boardman, Deere & Co. Technical Center
Dr. Marvin McKimpson, Michigan Technical University
Dr. Peggy Payne, Boise Cascade Corp., Wallula, WA
Dr. Alan Buchanan, Brunner & Lay Inc, Springdale, AR

Project Objective

The purpose of this project is to establish a framework from which to support future commercialization efforts of a new class of ultra-hard materials based on $AlMgB_{14}$. This framework is based on fundamental research into the compositional and processing variables that affect performance and efficiency in a wide-range of cutting, grinding, and wear resistance applications in the mining, forest products (mechanical pulping), metalcasting, and agriculture sectors. Along with our industrial partners, we are devloping and evaluating working prototype cutting and grinding inserts. Also under study is the technology for applying thin- and thick-film coatings of ultra-hard boride on various substrate materials.

Research approach

It is our intent for this research program to be dynamic and responsive to feedback from industrial partners. Consequently, adjustments in specific research priorities have been implemented, relative to the initial project roadmap. For example, the need to develop large-scale processing methods for this material is paramount, because the entire array of subsequent applications research is dependent on the availability of large numbers of samples. Consequently, a significant amount of effort has been directed toward this and other processing-related areas. Our approach remains consistent with the overall philosophy of investigating and identifying potential applications for this new class of ultra-hard material, while studying the fundamental mechanisms responsible for its remarkable behavior.

Background

Previous attempts to develop new superhard materials focused exclusively on *intrinsic* hardness, a material property that is a function of the chemical bonding environment, atomic arrangement in the unit cell, and to a lesser extent, atomic size. Commonly acknowledged ultra-hard materials such as diamond and cubic boron nitride fall in this category, as do most of the currently studied candidates such as C_3N_4 and α-Si_3N_4. However, only quite recently has attention turned to the role that ***extrinsic*** factors, e.g., microstructure, play in determining hardness and wear resistance. In 1999 Ames Laboratory scientists discovered that the microhardness of chemically-modified, ultrafine-grained icosahedral boride compounds can exceed 45 GPa, placing these materials in the super-hard category. A family of composites based on this material has been developed at Ames Laboratory, and characterized for hardness, microstructure, fracture toughness, and cutting performance against industrial materials of interest such as titanium, 304 stainless steel, concrete, graphite, and Inconel.

Cutting performance of tool specimens fashioned from hot pressed $AlMgB_{14}$ was evaluated by analysis of mass change (removal rate), wear mechanisms, surface chemistry (reactivity), and fracture mechanisms. Preliminary results indicate that this new family of materials exhibits good performance, while combining favorable toughness with minimal tool heating, leading to reduced wear and anticipation of long life. Efforts to scale-up processing from laboratory-scale quantities (e.g., 1 to 5 grams/batch) to pilot-plant industrial-scale (e.g., kilograms) constitute a major focus of this program. Pulsed laser deposition has also been employed as a convenient method for preparing thin film coatings of the ternary compound on substrates for characterization of composition and wear behavior. Moreover, in response to recent input from industrial partners on this program, a new research effort has been initiated with the objective of developing appropriate chemical modifications to the baseline boride composition to improve high temperature oxidation resistance.

Summary of Tasks

This report summarizes work performed from October 1, 2002 through September 30, 2003, as described in the four quarterly reports. Research focus areas receiving primary attention during this period include processing/scale-up, oxidation studies, cutting tests, and binder phase development. Progress in each area is summarized below.

Processing and scale-up studies

Processing

Achieving full density in ceramic materials is a long-standing processing challenge. The lack of plastic flow gives rise to exceptionally large activation energies for granule rearrangement. Conventional uniaxial hot pressing of mechanically alloyed $AlMgB_{14}$ powder results in compacts with densities of 95 to

96 percent; the residual 4 to 5 percent porosity having a significant deleterious effect on hardness and wear resistance. In order to investigate the expected benefits of overcoming this challenge, a sample of $AlMgB_{14}$ was ground, mixed with 15 volume percent of a metal binder phase, and shock-consolidated to full density by one of our industrial partners. The resulting cermet possessed a microhardness of ~ 30 GPa (typical for baseline – or undoped – $AlMgB_{14}$) with a plane strain fracture toughness of ~ 10 MPa-$m^{0.5}$. This is an extraordinary combination of hardness and toughness, surpassing by a considerable margin the performance of cemented carbide tools (~ 18 to 20 GPa and ~ 7 to 10 MPa-$m^{0.5}$). In general, as the hardness of a material increases, its fracture toughness (or resistance to failure by crack propagation) decreases proportionately. The existence of an inverse relationship between hardness and fracture toughness was discussed in a seminal paper by Viswanadham and Venables in 1977 [1].

Industrial applications involving use of hard and wear resistant materials are faced with a set of conflicting requirements. For example, in the metal casting industry, metal removal tools must possess sufficient toughness to withstand initiation of a cut without fracture or damage to the cutting edge. The tool must also possess a sufficiently high hardness (directly related to wear resistance) to overcome the variations in localized hardness in the workpiece material resulting from residual stress during cutting. If the material's toughness is increased beyond a certain point, wear resistance suffers, and tool life is dramatically reduced. Conversely, if the hardness is increased, wear resistance generally improves, but the probability of tool failure due to fracture increases dramatically. Moreover, these limitations are exacerbated in the severe environments observed during high speed machining and milling and, in particular, in the area of dry machining. Figure 1 offers a relative comparision of toughness and wear resistance among the most common tooling materials currently in existence, and shows the approximate region that optimized $AlMgB_{14}$-based materials are projected to occupy. As the ideal material simultaneously possesses both high wear resistance and toughness, the recently-observed values for fully-dense $AlMgB_{14}$ + binder place this material singularly in an important region previously unattainable by conventional materials.

Ceracon, Inc. (Carmichael, CA) has agreed to participate in a study of the feasibility of applying quasi-isostatic forging to the densification of $AlMgB_{14}$ particulate blended with various binder materials. A series of $AlMgB_{14}$ cermets mixed with Co, Ni, and the recently-developed Co-Mn binder have been prepared by grinding and sieving hot pressed compacts of the boride, blending with binder powder, and cold pressing into green articles. The green bodies will be isostatically forged and returned to Ames for microstructural and mechanical characterization during FY'2004.

[1] A Simple Method for Evaluating Cemented Carbides", Metallurgical Transactions A, Volume 8A, January 1977, pages 187-91

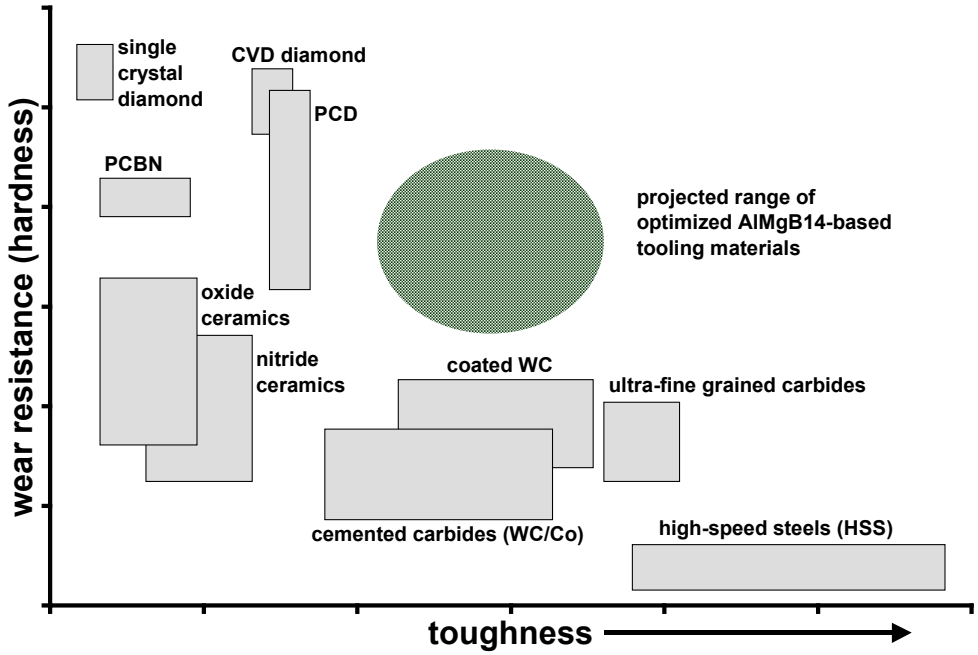

Figure 1. Relative comparison of toughness and wear resistance among current industrial tooling materials. (Projected region occupied by optimized $AlMgB_{14}$ is based on recent densification studies.)

Distribution of TiB_2 reinforcement phase

Realization of the optimum hardness and fracture toughness in this or any ultra-hard *extrinsic* composite depends on the ability of a processing technology to distribute a nanoscale reinforcement phase phase uniformly throughout the material. Moreover, the reinforcement phase must be compatible with the hard matrix phase, that is, it must possess appropriate elastic moduli, density, surface energy, and chemical stability. Non-uniformity in the distribution of reinforcement phase results in localized strain gradients and concomitant fracture and premature failure of the material. $AlMgB_{14}$-based specimens possessing the highest hardness observed to-date, 45 to 50 GPa, have possessed a microstructure similar to that shown in figure 2a, where it is seen that the distribution of sub-micron TiB_2 reinforcement phase (lighter regions) is reasonably uniform within the $AlMgB_{14}$ matrix (darker regions). The precursor MA powder, shown in figure 2b, is itself nanoscale, and highly homogeneous.

In contrast, incomplete or improper comminution and mixing of the reinforcement phase with $AlMgB_{14}$ powder, as illustrated by the extreme example in figure 3, results in no net improvement in hardness over that of the baseline $AlMgB_{14}$ material. In this example, commercial TiB_2 powder (-325 mesh) was added to mechanically alloyed $AlMgB_{14}$ powder, and the composite was milled for an

additional 30 minutes. It is clear from the figure that the TiB_2 platelets had not undergone any appreciable degree of comminution during the 30 minutes of milling.

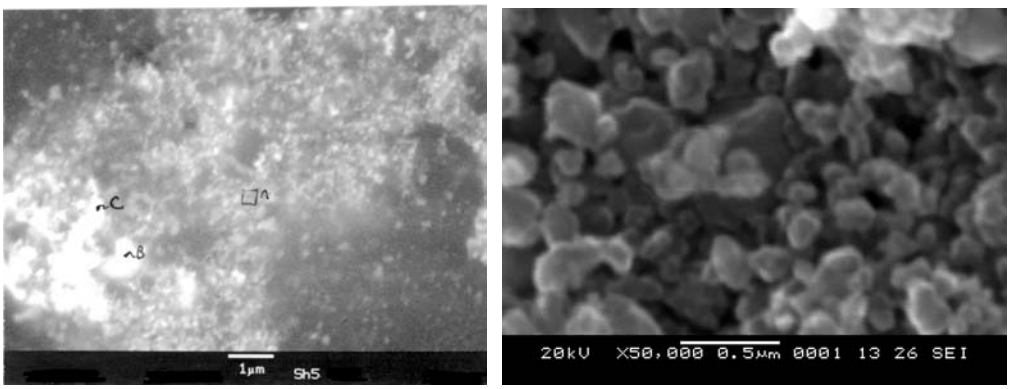

Figure 2. (a) microstructure of hot pressed articles possessing extreme hardness (SEM – BSE mode), (b) precursor particle morphology after MA

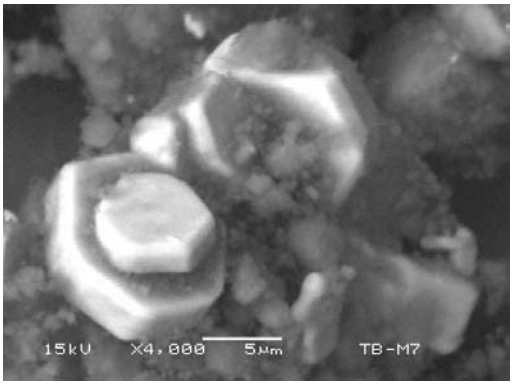

Figure 3. An example of incompletely-comminuted TiB_2 (bright platelets) after mixing with $AlMgB_{14}$ MA powder. (note the comparatively large size of the TiB_2 platelets, leading to no net improvement in hardness)

In order to establish a reproducible mixing technique amenable to large-scale processing, a series of experiments was initiated involving a solution-chemistry approach. The motivation was to improve reproducibility in reinforcement particle size and morphology by first mechanically alloying elemental titanium and boron to form nanoscale TiB_2. The next step was to add an appropriate amount of the nanoscale TiB_2 to a charge of mechanically alloyed $AlMgB_{14}$, and then to disperse the entire mixture in a solution of hexane (C_6H_{14}). The solutions were magnetically-stirred for varying amounts of time, and the dispersed particles were allowed to settle onto a 30 nm filter. Excess hexane was decanted, and the residual fluid was allowed to evaporate overnight in a vacuum desiccator. The

resulting distribution of TiB_2 was examined in a SEM in backscattered mode. As shown in figure 4, a significant reduction in average size of the TiB_2 was achieved, compared with addition of commercial TiB_2 powder, and no particle was found to be larger than ~ 1 micron. (The lighter-contrast areas in the figure correspond to TiB_2, as determined by energy-dispersive x-ray analysis.)

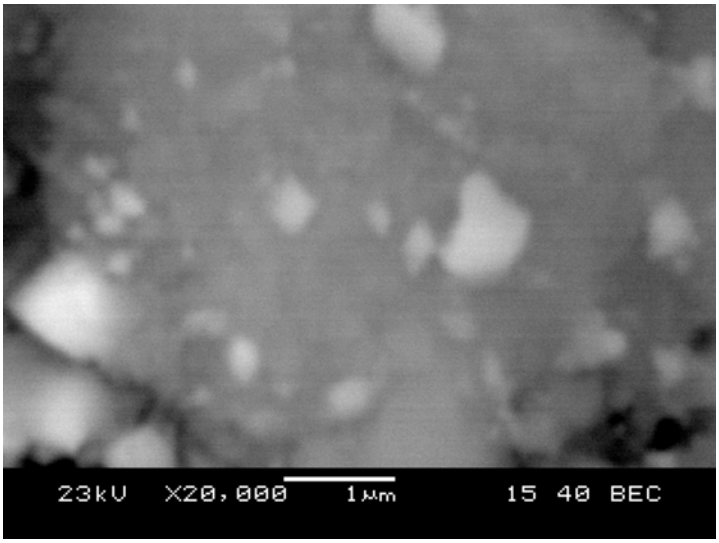

Figure 4. BSE micrograph of Zoz-milled $AlMgB_{14}$ powder mixed with TiB_2 in hexane
(lighter-contrast regions correspond to TiB_2 particles)

Additional experiments, to be expanded during FY'2004, will optimize this process with the goal of minimizing both particle size and standard deviation. The process holds great promise for generating a uniform distribution of reinforcement phase particulate on an industrial scale. A larger quantity of ($AlMgB_{14}$ + TiB_2) will be prepared by the solutionizing approach, and the resulting powder will be hot pressed to verify the beneficial effect on microhardness.

Scale-up

High-energy milling is an essential component of the processing of these alloys, in order to produce the ultra-fine grain size required for the extrinsic hardness effect. Installation of a high-energy Zoz attritor mill was completed early in FY 2003, and preliminary milling trials were initiated shortly thereafter. This device generates a sufficient energy density to achieve comminution equivalent to that in the small-scale Spex mill, but with significantly larger quantities of powder (400 grams vs. 5 grams); thus, it constitutes an important step in the scale-up effort to produce kilogram-quantities of new ultra-hard, wear resistant materials.

The Spex 8000 and the Zoz CM-01 produced similar degrees of comminution of the precursor Al, Mg, and B, as shown by x-ray diffraction patterns of their corresponding MA powders in Figure 5. In both cases, a considerable amount of particle size refinement is observed, as indicated from the peak broadening; in addition, partial alloying of the constituents has occurred.

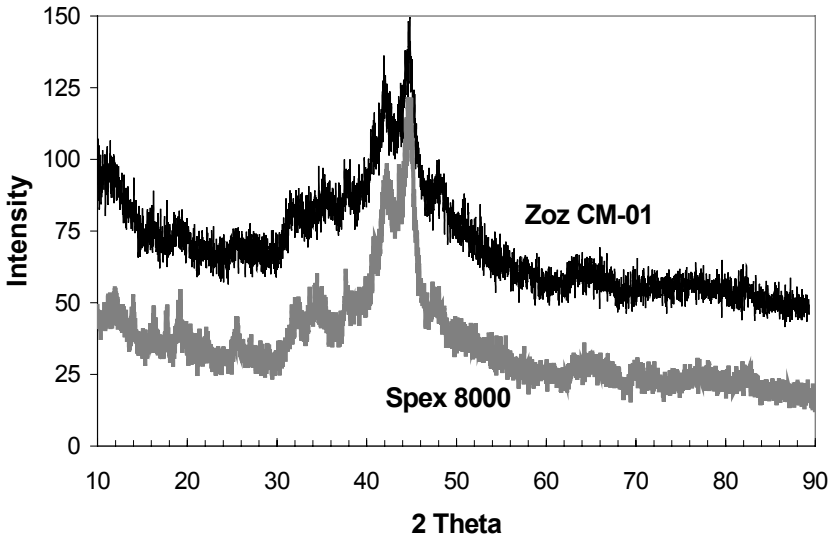

Figure 5. X-ray diffraction pattern of $AlMgB_{14}$ powder produced by a research-scale Spex 8000 (lower curve), and by the pilot plant-scale Zoz CM-01 (upper curve). Note the similarity, showing that both devices produce similar results.

A study was also performed to ascertain the relative *rates* of comminution in the Spex and Zoz equipment. In order to optimize processing of $AlMgB_{14}$ and related compounds for eventual commercialization, it is necessary to identify the point at which sinterability of powders produced by the large-scale equipment becomes comparable to that of the control group, which in this case is the Spex-milled powder. When comparing the X-ray diffraction patterns of $AlMgB_{14}$ powder taken from the Zoz mill at various intervals, shown in Figure 6, it can be seen that the 3 hour diffraction pattern of the Zoz-milled material is nearly identical to the pattern corresponding to 12 hours of Spex milling. The higher rate of comminution in the Zoz mill is significant in terms of processing throughput and of minimizing the amount of media wear debris and contamination in the powder.

The morphology of powders produced by high-energy milling in the Zoz CM-01 after 1 and 16 hours of comminution is shown in figure 7. The nominal 44 micron starting material is reduced in size to the 10 to 20 micron range after 1 hour of cyclic milling. The competing processes of fracture and cold welding result in a bifurcation in size distribution, with micron- or sub-micron particles coexisting with larger 20+ micron agglomerates.

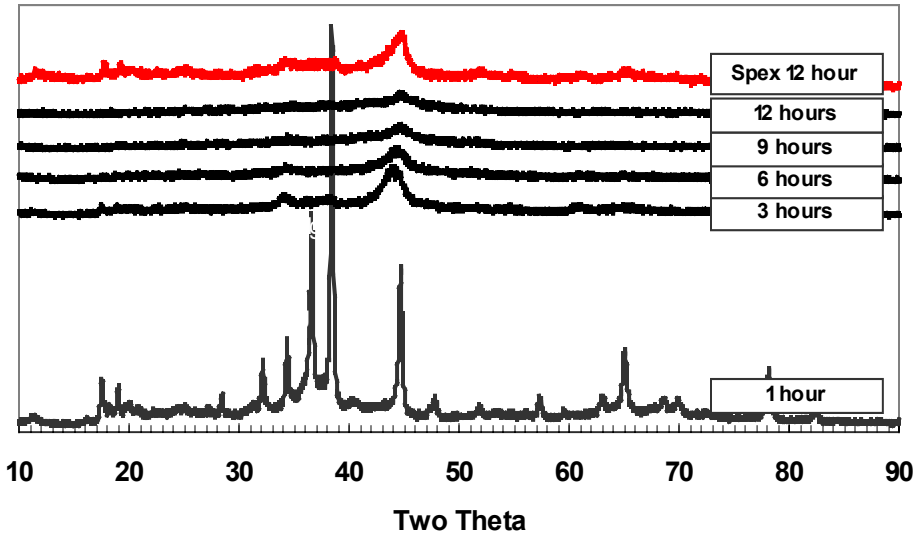

Figure 6: X-ray diffraction patterns of $AlMgB_{14}$ powders milled in Zoz CM-01 compared to Spex milled powder with standard ball loading. (Note that the 12-hour Spex pattern exhibits roughly the same degree of peak broadening as that of the 3 hour Zoz-milled powder)

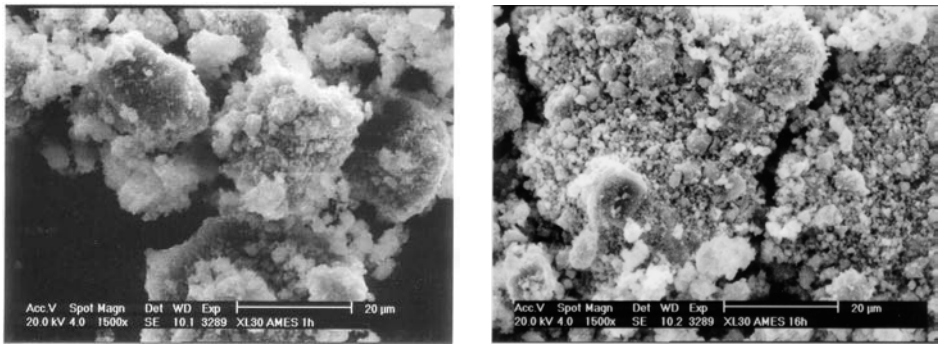

Figure 7. Morphology of $AlMgB_{14}$ powders obtained from 1 hour (left) and 16 hours (right) of high-energy milling in the Zoz CM-01.

The MA powder is consolidated into dense articles by inert gas hot pressing at 1400°C. Hot pressing completes the diffusion reaction initiated by mechanical alloying, and produces the desired 1:1:14 structure as the primary phase. When the x-ray patterns of hot pressed $AlMgB_{14}$ prepared by a Spex 8000 and by the Zoz CM-01 are compared, both devices are observed to produce the 1:1:14 as the dominant phase. However, as seen in figure 8, the pattern corresponding to material prepared in the CM-01 exhibits stronger diffraction peaks for the impurity spinel phase, of which one such peak is shown at $2\theta \approx 19°$. Spinel ($MgAl_2O_4$) is

the thermodynamically favored phase in an oxygen-containing environment. The relative volume fraction of spinel in different 1:1:14 samples can be taken as a qualitative indicator of the amount of oxygen present, either from the precursor materials or from the processing environment. TEM studies are planned during FY'2004 in order to determine the size and distribution of spinel in the CM-01 materials, and its effect on hardness, wear resistance, and fracture toughness.

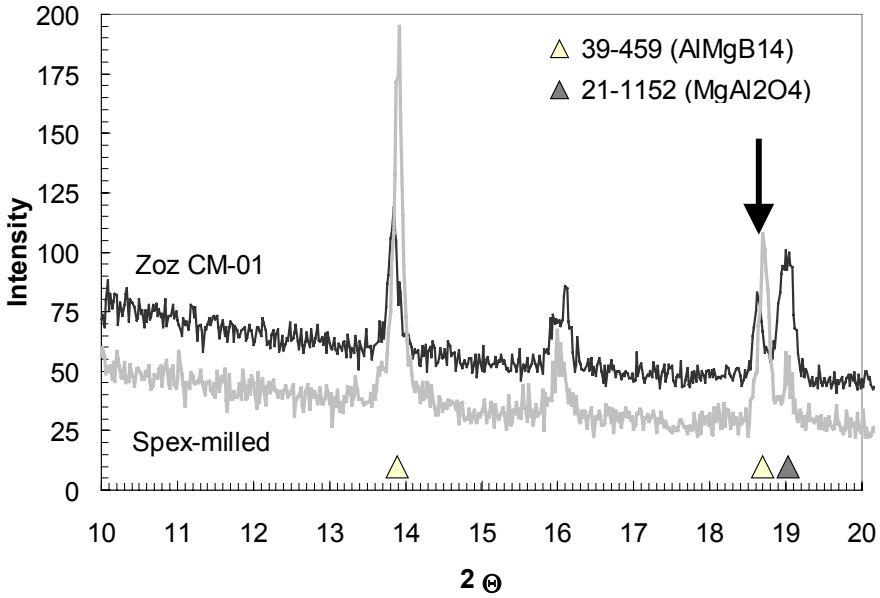

Figure 8. X-ray diffraction patterns of hot pressed $AlMgB_{14}$ using MA powder prepared in a Spex 8000 (lower curve) and Zoz CM-01 (upper curve). Note the higher intensity spinel peak corresponding to the powder milled in the CM-01 (indicated by the arrow).
(An iron borate impurity phase peak occurs at $2\theta = 16.2°$)

Another important processing variable is the quantity of second phase iron resulting from solid state comminution processing of the precursor materials. The presence of a small amount of Fe has not been found to have a deleterious effect on hardness of the borides; in fact, it is believed that a few percent Fe facilitates densification during hot pressing and contributes to fracture toughening by forming a comparatively ductile secondary phase. However, as one would expect, excessive amounts of iron result in a precipitious decrease in hardness as the percolation threshold is approached. Consequently, it is important to characterize the amount of Fe contamination resulting from various comminution techniques and to establish a process control specification for future commercialization efforts. To this end, samples of as-milled boride were removed after processing in three different types of comminution devices, a low-energy planetary mill (Fritsch P-5), a high-energy vibratory mill (Spex 8000), and a high-energy attritor mill (Zoz CM-01). The

samples were characterized for Fe content by ICP-AES and the results are summarized in figure 9.

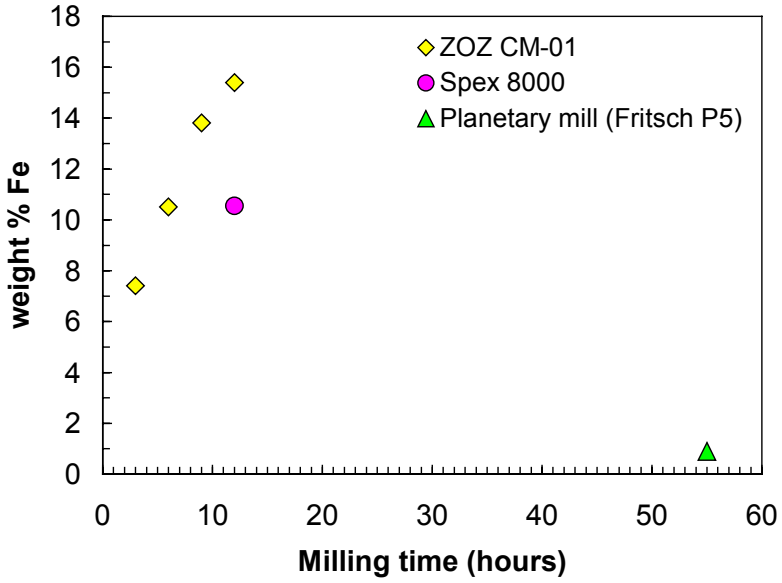

Figure 9. Comparison of Fe pickup in powdered $AlMgB_{14}$ samples prepared by three different solid state comminution techniques.

The total amount of Fe contamination after 6 hours of milling in the Zoz CM-01 was found to approximately equal the amount present after 12 hours of Spex milling. Note the significantly lower amount of Fe contamination in the planetary milled material, despite the longer processing time. These results are directly related to the average kinetic energy per impact in each device. The implication for commercialization processing is that high-energy attrition milling must be limited to no more than 6 hours.

Oxidation behavior

In response to a suggestion from one of our industrial partners, the high-temperature oxidation resistance of $AlMgB_{14}$ has been added as an additional research component on this project. Conventional hard materials such as diamond and cubic boron nitride lack sufficient oxidation resistance at temperatures above 1000°C to serve as useful abrasives in severe environments. Currently, Al_2O_3 is the material of choice in high temperature applications requiring hard materials, albeit its hardness versus temperature curve drops precipitously above ~700°C. In more complex materials such as $AlMgB_{14}$, the large number of atoms per unit cell, coupled with incompletely occupied metal sites, gives rise to additional degrees of freedom with respect to atomic substitution. Isothermal oxidation tests on $AlMgB_{14}$ at 1000°C in static air

revealed that the compound forms a *non-protective* B_2O_3 oxide scale. Lateral flow of the boric oxide continually exposes substrate material, resulting in linear oxidation kinetics. The goal is to design a material based on the same orthorhombic crystal structure as $AlMgB_{14}$, but with appropriate substitution of an element that would facilitate formation of a protective oxidation scale at high temperatures. One approach consists of partially or completely replacing Mg with Cr to form $Al(Mg_{1-x}Cr_x)B_{14}$. Because of the large negative free energy of formation of B_2O_3 (-1194 KJ/mol), it is doubtful that this oxide will be completely replaced in the resulting scale. However, if a sufficient volume fraction of a higher viscosity, protective oxide former is added, the resulting mixed oxide (e.g., $B_2O_3 + Cr_2O_3$) may provide adequate protection for reasonable lengths of time.

Initial samples for this study were prepared with a nominal composition of $AlCrB_{14}$, which was subsequently found to form a nanoscale composite of $CrB_2 + AlB_{12}$ after inert-gas hot pressing. During a 1000°C isothermal oxidation heat treatment, the composite partially transformed to the desired $AlCrB_{14}$ phase, plus additional minor phases of Cr_2O_3, B_2O_3, and $Al_4B_2O_9$. The room temperature Vicker's hardness of this composite was found to equal 30 GPa with a 1000 g_f load, which is comparable to that of the baseline $AlMgB_{14}$ composition. The oxidation resistance of a hot pressed sample of this material was determined by measuring the weight change following a 100 hour isothermal soak at 1000°C in static air. No evidence of a reaction between the sample and the alumina crucible used to contain it was found. A thin oxide coating formed on all exposed surfaces, which gave rise to a specific mass gain of 5 mg/cm^2.

Additional samples were prepared with partial substitution of Cr for Mg, in the form $Al(Mg_xCr_{1-x})B_{14}$, where x = 0.9, 0.8, 0.7, 0.5, and 0 in order to determine the range of chromium compositions forming the orthorhombic I_{mam} structure in the as-hot pressed condition (i.e., without a post consolidation heat treatment). A portion of the x-ray diffraction pattern obtained on a heat-treated $AlCrB_{14}$ specimen (containing no Mg) is shown in Figure 10, which is compared with a pattern from a sample of as-hot pressed material and also with the calculated peak positions. (The calculated diffraction patterns for the orthorhombic $AlMgB_{14}$ and $AlCrB_{14}$, assuming full occupancy, show negligible difference within the 2-Θ range and scaling factor indicated in the figure.)

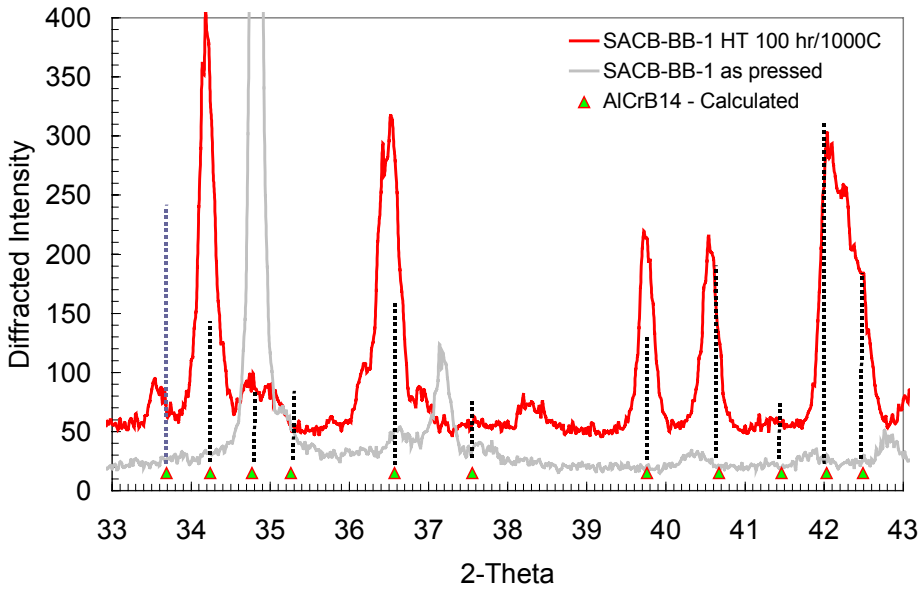

Figure 10. X-ray diffraction pattern of $AlCrB_{14}$ before (light gray) and after (dark) a 100 hour heat treatment in air at 1000°C. Peak positions corresponding to the calculated diffraction pattern for orthorhombic $AlCrB_{14}$ are shown for comparison.

Figure 11 compares the diffraction patterns obtained on a number of the partially-substituted compositions. There is evidence that the x=0.9 and x=0.7 compositions did form the 1:1:14 structure during MA and hot pressing. It appears less certain that the higher Cr-content compositions formed the desired phase without the benefit of a secondary heat treatment. That a heat treatment appears necessary to transform the material into the desired phase may be an indication of limited solubility for Cr in the orthorhombic structure due to its comparatively small atomic radius and resulting lattice strain (0.125 nm vs. 0.160 nm for Mg). During oxidation, it is speculated that diffusion of Cr atoms to the surface depletes the bulk of Cr, relaxing the lattice and favoring formation of the reduced-occupancy structure. Future planned work includes an assessment of site occupancy of the various atomic species by performing a full-profile Rietveldt analysis of the x-ray patterns. In addition, compositions and heat treatments will be optimized in order to obtain the most favorable combination of hardness and oxidation resistance. The temperature dependence of hardness will be measured on selected samples.

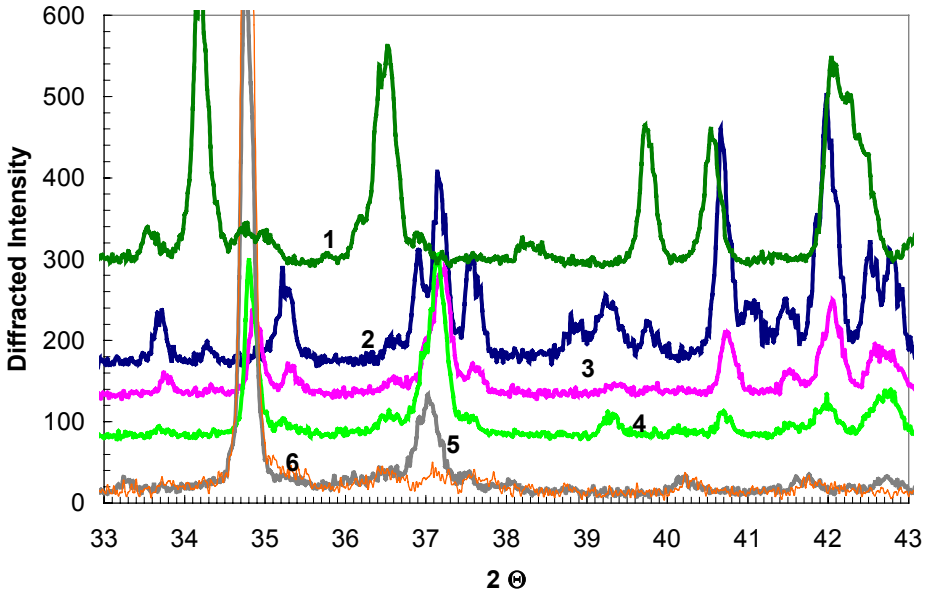

Figure 11. X-ray diffraction patterns of various boride samples and corresponding calculated peak positions at 273K. (The strong line at 34.8° corresponds to CrB_2.)
Key:

1 = $AlCrB_{14}$ (heat treated 1273K for 100 hours in air)
2 = $Al(Mg_{0.9}Cr_{0.1})B_{14}$
3 = $Al(Mg_{0.7}Cr_{0.3})B_{14}$ 5 = $Al(Mg_{0.25}Cr_{0.75})B_{14}$
4 = $Al(Mg_{0.5}Cr_{0.5})B_{14}$ 6 = $AlCrB_{14}$ (as-pressed).

Cutting and wear tests

Previous metal cutting tests have shown that fully-dense, homogeneous tooling samples of $AlMgB_{14}$ can be successfully employed in high-speed metal removal applications under environmentally-friendly (dry) conditions. The performance of these materials against a number of industrially-important metals and alloys has been evaluated; in particular, semi-quantitative tests have been performed on 304 stainless steel, Inconel, 6061 aluminum, and recently, Ti-6Al-4V. Titanium alloys such as Ti-6Al-4V are of considerable interest to the aerospace, automotive, and biomedical industries because of their high strength-to-weight ratio and excellent corrosion resistance. Unfortunately, these alloys are difficult to machine because of their inherent high chemical reactivity and comparatively low thermal conductivity, which results in large thermal fluxes directed into the tool, exacerbating wear mechanisms and drastically reducing tool life. It is among the Ti-group of alloys that the need for improved tooling materials is most urgent, and where significant short-term progress with $AlMgB_{14}$ appears most promising.

The extent of chemical reactivity between baseline $AlMgB_{14}$ and Ti-6Al-4V at temperatures typically encountered during high-speed machining was the subject of a study performed by the subcontractors on this project at the University of Arkansas. This study involved a series of diffusion experiments, consisting of pressing the two materials together and heating the couple for 120 hours at 1000°C (1800°F), a temperature typically observed at the tool-workpiece interface. The composition profiles were obtained using an Electron Probe Microanalyzer (Model JXA-8200) at Oak Ridge National Laboratory's High Temperature Materials Laboratory. Prior to diffusion testing, the microhardness and wear resistance of hot pressed baseline specimens (i.e., with no dopants or additive) were characterized. A Calo-wear testing technique was employed to determine abrasion resistance, in which a 25-mm diameter spherical tungsten carbide ball is rotated against the tool. The sliding velocity was fixed at 500 rpm with a 0.5 N normal force acting on the specimen. The three-body abrasion was achieved by introducing a 5 μm diamond abrasive slurry. The size of craters imposed due to abrasion in the presence of hard abrasive particles is a function of wear coefficient. In addition, Vickers hardness was measured using a Zwick hardness tester at a load of 0.1kg. The results, summarized in Table 1, show that the wear coefficient (resistance to cratering by abrasion) is consistent with the measured microindentation hardness of the material.

Table 1: Results of Micro-indentation Hardness
and Three-body Abrasive Wear Tests
(lower values for wear coefficient are desirable)

Material	Microhardness, $HV_{0.1}$, GPa	Wear Coefficient ($m^2/N \times 10^{-15}$)
$AlMgB_{14}$ (baseline)	31	1.61
Al_2O_3-TiC	22	2.88
Al_2O_3-SiC_w-TiC	19	2.67
WC-Co	24	1.78

When the $AlMgB_{14}$/Ti-6Al-4V diffusion couples were inspected following a 120 hour heat treatment, it was observed that the borides did not bond to the work-piece alloy, and that the components could easily be separated. Figure 12 shows the interdiffusion zone of a typical diffusion couple. An elemental map of region B (dark gray) indicates the presence of titanium and boron, in what appears to be a titanium boride phase. The elongated gray phase in regions C and D are borides, mostly of titanium, but also containing small amounts of vanadium. The morphology of these borides suggests grain boundary diffusion of boron from the tool into the workpiece.

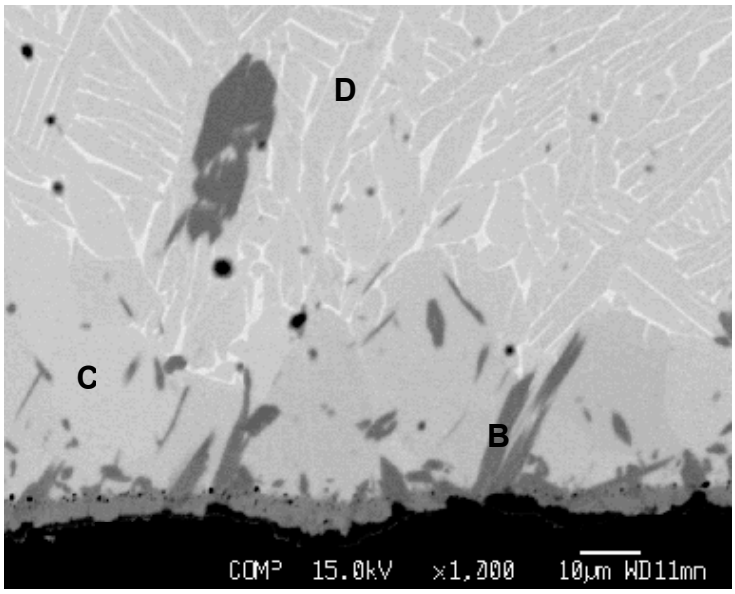

Figure 12. Reaction zone of Ti-6Al-4V after diffusion test with $AlMgB_{14}$ (Ti-6Al-4V is on the top and the $AlMgB_{14}$ is on the bottom)

The composition profiles resulting from this diffusion couple are shown in Figure 13. For ease of interpretation, the profiles of elements in the tool are shown separate from those of the work-piece.

The dominant diffusing species is boron, and its concentration into the work-piece material shows a periodicity that is matched by the variation in the titanium signal, suggesting the formation of a Ti-B phase. A more detailed observation of the concentration profile of vanadium shows that there is a depletion of vanadium within the interdiffusion zone towards the interface. This can be observed in Fig. 12 in the regions marked B and C, where the typical two-phase morphology of the α-β alloy is absent. The width of interdiffusion zone in the work-piece alloy can be estimated from the diffusion profile to be about 40 μm, which is considerably less than that observed in the WC-Co/Ti-6Al-4V couple (see below).

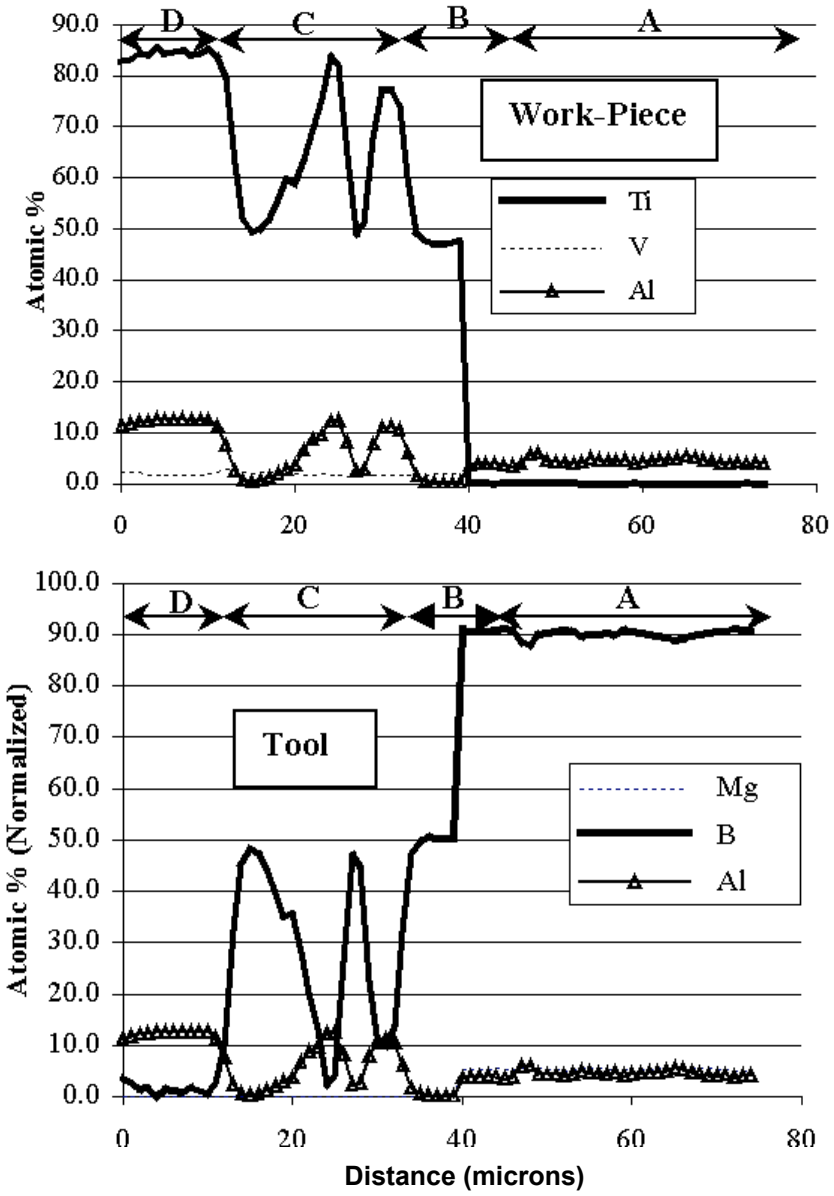

Figure 13. Compositional profiles of a $AlMgB_{14}$/Ti-6Al-4V diffusion couple after 120 hours at 1000°C.

A similar set of experiments was performed in which the diffusion characteristics of WC/Co and Ti-6Al-4V were evaluated. An SEM micrograph of a typical interdiffusion zone is shown in Figure 14, and the corresponding composition profiles are shown in Figure 15. The width of the interdiffusion region is

considerably larger in the WC/Co – Ti-6Al-4V couple than in the case of the $AlMgB_{14}$ tool, indicative of a strong affinity between the cemented carbide and the Ti alloy.

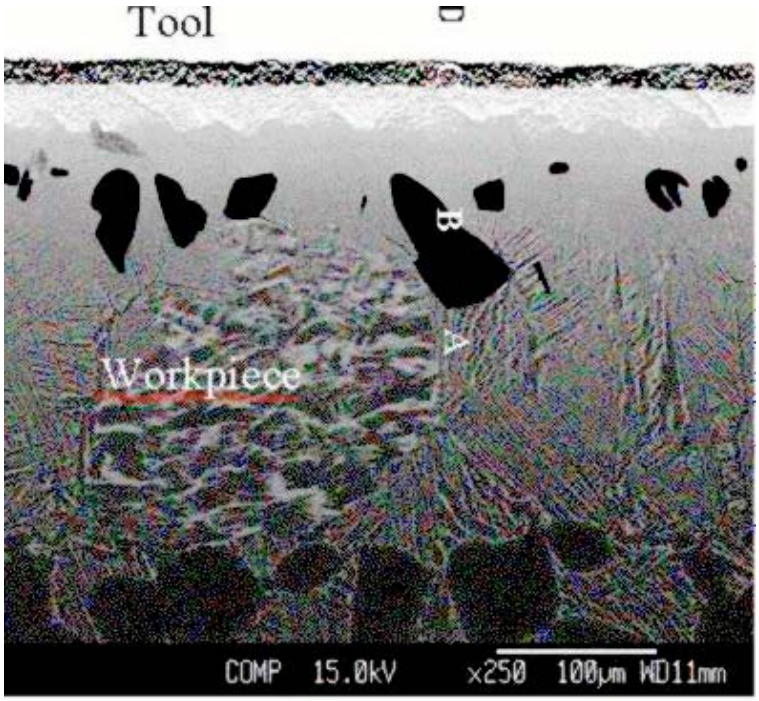

Figure 14. SEM micrograph of a typical reaction zone between WC/Co ("Tool") and Ti-6Al-4V ("Workpiece") after a 120 hour heat treatment at 1000°C.

The most striking microstructural features are the islands of Ti-C particles, which correspond to $Ti_{0.6}C_{0.4}$. These islands of titanium carbide form all along the interface in a regular manner, and vary in size from a few microns to over 100 microns. The strong chemical reactivity of Ti leads to a decomposition of WC and subsequent rapid grain boundary diffusion of carbon, which subsequently reacts with titanium. An increased concentration of cobalt was also observed near the interface, suggesting the formation of the eta phase at the tool surface.

Another interesting feature of this diffusion couple is that there is a clear indication of Ti diffusion into the tool surface, with formation of a (W,Ti)C phase. This is a thermodynamically stable phase, often observed in TiC-coated cemented carbide tools. The diffusion profile in this region shows a variation in the concentration of Ti and W, indicating that Ti can diffuse below the surface of the tool to a considerable distance.

This study concluded that $AlMgB_{14}$ exhibits a very high hardness and wear resistance, as compared to other alumina-based cutting tools, including Al_2O_3-

TiC, and the SiC whisker-reinforced Al_2O_3-TiC. In addition, it was experimentally determined that $AlMgB_{14}$ is less reactive with titanium alloys than conventional cemented carbide cutting tools.

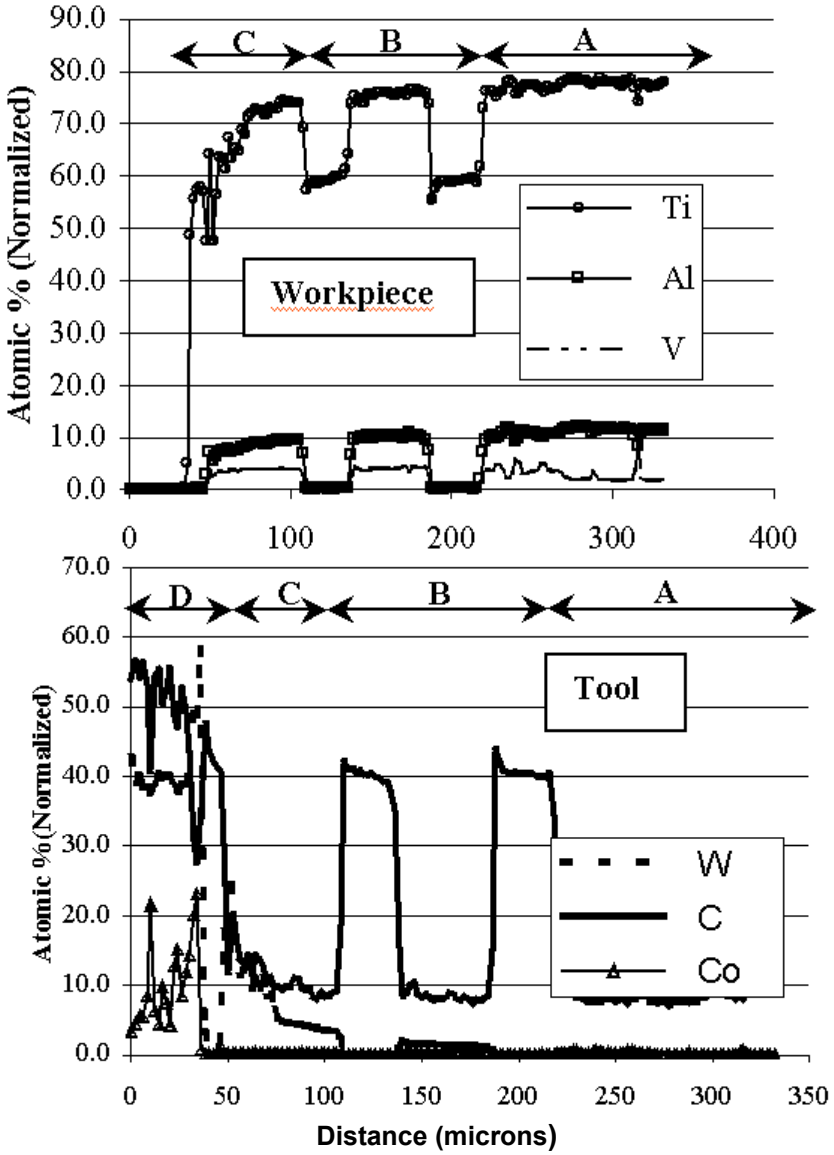

Figure 15. Compositional profiles of a WC/Co +Ti-6Al-4V diffusion couple (120 hrs, 1000°C).

In addition to the diffusion studies, tribology studies on various $AlMgB_{14}$ compositions were also performed at Iowa State University and at the University of Arkansas. The objective was to determine how the various powder comminution routes affect the wear resistance of the consolidated compact. To

this end, a series of low-speed single point scratch tests using a Rockwell diamond indentor were employed in order to compare the abrasion characteristics of boride material prepared by three different comminution techniques: low-energy planetary milling (Fritsch P-5), high-energy vibratory milling (Spex 8000), and high-energy attritor milling (Zoz CM-01). Resistance to scratch abrasion by a diamond indenter is inversely proportional to the volume of material removed which, in turn, is directly related to the area under the profilometer curve of surface roughness versus position. The boride samples that were tested each contained 3 to 4 percent porosity, which is known to have a deleterious effect on wear resistance. Earlier studies demonstrated that residual porosity originating from powder agglomerates significantly lowers a material's abrasive wear resistance. The results, shown in figure 16, indicate that samples prepared by planetary milling possess the lowest scratch resistance at all loads, while those prepared from Spex and Zoz exhibit significantly better resistance to scratching. In general, planetary-milled samples contain the highest amount of residual porosity, which can, in most circumstances, be eliminated by a final isostatic densification step. Samples prepared with TiB_2 second phase reinforcement gave results that were superior to all other materials

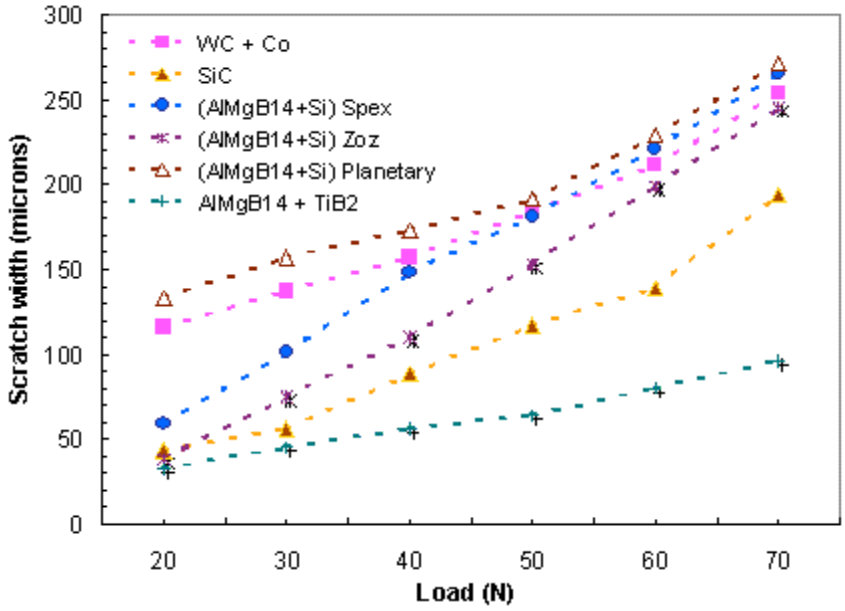

Figure 16. Single-point scratch tests of various hard materials using a Rockwell diamond indentor.

Binder phase development

Advanced materials for metal removal applications must possess both good hardness and fracture toughness. Tungsten carbide (WC) is moderately hard but

also quite brittle; addition of Co as a binder phase enables monolithic tools fashioned from this material to better tolerate impacts such as those encountered during discontinuous cutting that would otherwise result in fracture and loss of the tool. WC cermets with Co additions in the range of 3 to 13 weight percent are employed for machining cast iron, non-ferrous metals, and non-metallic materials, but generally not for machining steels [16]. Grades containing up to 25 weight percent binder phase are normally used for non-machining, high impact applications of cemented carbides. Hardness decreases with increasing Co content and with increasing WC particle size. Cemented carbides are prepared by liquid phase sintering with a liquid phase eutectic of C and Co which is formed at 1320°C at a composition of 11.6 at. % C. The WC/Co composite is therefore a classic metal-ceramic composite, a hard and brittle material dispersed in a continuous ductile matrix. This section summarizes research efforts to develop a new binder phase, suitable for use with $AlMgB_{14}$.

Addition of ~17 atomic percent Mn to Co produces an alloy with a liquidus temperature of ~1375° C. Consequently, a mixture of Co-Mn and $AlMgB_{14}$ could be hot pressed at 1400°C, sintering the boride in a continuous binder phase. At equilibrium Mn has extensive solid solubility in Co, and stabilizes FCC α-Co.

For well developed cracks, where the crack length, *C*, is much greater than the indentation diagonal length, a, the plane strain fracture toughness may be estimated as:

$$K_{ic} = x\left(\frac{E}{H}\right)^{\frac{1}{2}}\left(\frac{P}{C^{\frac{3}{2}}}\right) \quad (1)$$

In the above equation, *E* is the material's Young's modulus, *H* is the Vickers hardness (Kg/mm^2), and *P* is the applied load (Newtons). Variable *x* is a material constant, which has been shown to equal 0.016 in calibration studies with a wide range of materials. Typical values for fracture toughness in a variety of materials are shown in Table II. As indicated, fracture toughness values for ceramic materials are inherently low, typically less than 4 MPa√m, whereas the more ductile metallic alloys tend to possess K_{IC} values greater than 20 MPa√m. A reasonable goal for the $AlMgB_{14}$-based materials is a K_{IC} value similar to those of current-generation cemented carbide tools, or around 7 to 9 MPa√m.

The mechanical properties of two samples of a Co-Mn alloy were characterized by a series of standard tensile tests (ASTM E8) on samples machined from hot-swaged rod. An arc-melted finger of the Co-Mn alloy was placed into a stainless steel tube and hot swaged to a 15% reduction in cross sectional area at 700ºC in order to achieve hot break-down of the arc melted grain structure. Tensile specimens identified as CoMn1 and CoMn2 were pulled at strain rates of 5.0 (10^{-4}) s^{-1}, and 1.2 (10^{-4}) s^{-1} respectively. A traveling microscope was used to

measure % reduction in area ductility data. The resulting engineering stress – strain plots for the binder alloy are shown in Figure 17, which indicate that the Co-Mn alloy possesses ultimate tensile strength of 670 MPa combined with unusually high ductility of 40% or more elongation. These values are presented in Table III in comparison with strength and ductility values from the literature for pure Co.

Table II: Fracture Toughness of Selected Materials (22°C) [14,15].

	K_{IC} (MPa√m)
Aluminum oxide	3.9
Concrete	0.2 - 1.4
Diamond (natural)	3.4
Glass (borosilicate)	0.8
Silicon nitride (sintered)	5.3
Ti - 6Al - 4V	44 - 66
Aluminum alloy (7075-T6)	24
B_4C	3
WC + Co	7.5 - 8.9

Results of these initial studies show that the Co-Mn binder phase is a strong, highly ductile alloy compatible with the ultra-hard boride material, meaning that the binder becomes liquid at the hot pressing temperature without adversely affecting the boride. It was observed that the binder phase increased the fracture toughness of the $AlMgB_{14}$, although a precise relationship between binder amount and K_{IC} has yet to be determined.

Tribology studies are in progress at both Iowa State University and at the University of Arkansas on a number of $AlMgB_{14}$ compositions; results will be summarized in subsequent reports.

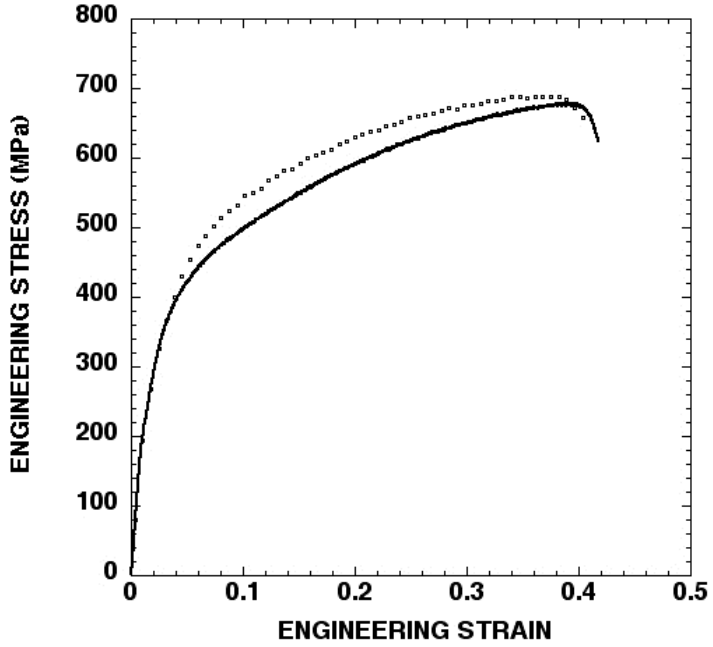

Figure 17. Room temperature stress – strain behavior of two specimens of Co-Mn hot swaged to 15% reduction in area at 700˚ C prior to testing. Tensile strain rates were 5.0(10^{-4}) s^{-1} (solid curve) and 1.2(10^{-4}) s^{-1} (dotted curve).

Table III - Room Temperature Ultimate Tensile Strength and Ductility of Co-Mn Compared with Literature Values for Pure Co.

	UTS (MPa)	Ductility (elongation)	Ductility (reduction in area)
Co-17%Mn: Tensile Specimen CoMn1 (strain rate 5(10^{-4}) s^{-1})	675	42%	40%
Co-17%Mn: Tensile Specimen CoMn2 (strain rate 1.2(10^{-4}) s^{-1})	685	40%	52%
Co, 99.9% purity, as-cast	235	4%	NA
Co, 99.9% purity, annealed	255	8%	NA
Co, 99.9% purity, cold-worked	690	8%	NA
Co, 99.6% purity	690	14%	16%
Co, 99.5% purity, hot-worked then annealed at 800˚ to 1000˚ C	800 to 875	15 to 30%	NA

Thin film coatings

Pulsed laser deposition (PLD) was employed as a preliminary means to study the deposition characteristics and physical properties of $AlMgB_{14}$ films on pre-oxidized silicon substrates during development of appropriate processing technologies to produce large-scale powder quantities suitable for thermal spray trials. The general arrangement and relative scale of the PLD films is shown in figure 18.

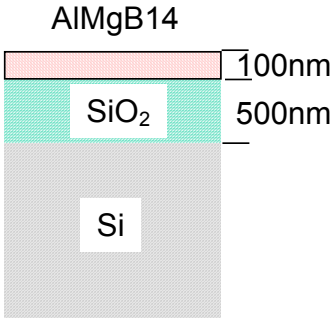

Figure 18. Arrangement of PLD-deposited $AlMgB_{14}$

The as-deposited films were typically 100 to 400 nm thick, and their X-ray diffraction patterns indicate an amorphous structure, that can be crystallized by annealing for two hours at 1000˚ C. The nanohardness of both amorphous and crystalline coatings was measured by nanoindentation and found to range from 30 to 40 GPa, with the crystalline films being slightly harder than the amorphous films, as shown in Figure 19. Subsequent nanoindenter measurements made on thicker films (400 nm) that had been deposited for 6 hours at 300˚ C, confirmed earlier results by giving hardness values ranging from 37 to 41 GPa.

Nanoindenter scratch tests were also performed on these $AlMgB_{14}$ coatings to determine the coefficient of friction in both the as-deposited and annealed condition. Results are shown in Figures 20a for the amorphous films and 20b for the annealed films. Boride films often form an extremely thin surface coating of $B_2O_3 + H_2O$ which has a very low coefficient of friction, and this appears to have occurred on these coatings; the measured coefficient of friction was only 0.05. An obvious application for these ultra-hard boride coatings would be a wear resistant, self-lubricating coating for Si MEMS components.

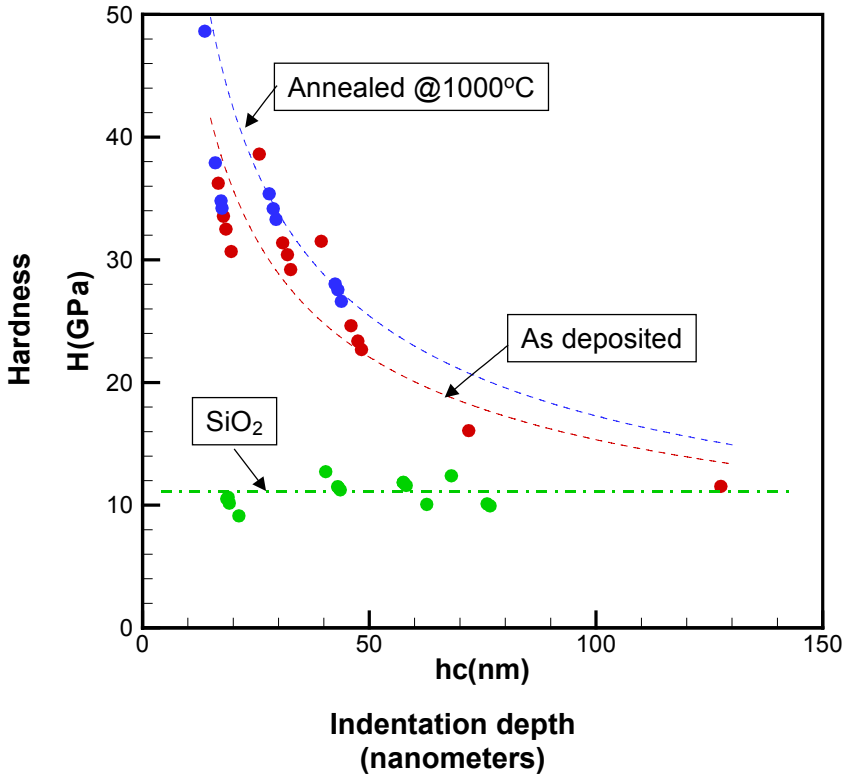

Figure 19. Hardness of $AlMgB_{14}$ film deposited by pulsed laser deposition as a function of Indentation depth.

Figure 21 shows a plan-view bright field TEM image of baseline $AlMgB_{14}$ film (i.e., sans TiB_2 reinforcement phase) deposited at 573 K. The selected area diffraction pattern (SADP) from this film is shown in the inset, in which a halo (diffuse) rings pattern is clearly evident. Furthermore, static and conical dark field images show no evidence of a nanocrystalline structure, indicating that the film is mostly amorphous; energy dispersive spectroscopy showed a homogeneous film composition across the bright and dark stripes of the apparent maze pattern. It was speculated that the observed maze pattern might be caused by variation in film thickness, possibly a consequence of non-uniform contraction of the $AlMgB_{14}$ upon cooling from 573 K due to thermal expansion mismatch between the Cu grid and amorphous $AlMgB_{14}$ film. The TEM image and SADP of $AlMgB_{14}$ film deposited at room temperature are similar to those of 573 K-deposited $AlMgB_{14}$ film, except that the former does not show the maze pattern, indicative of the amorphous structure in this film.

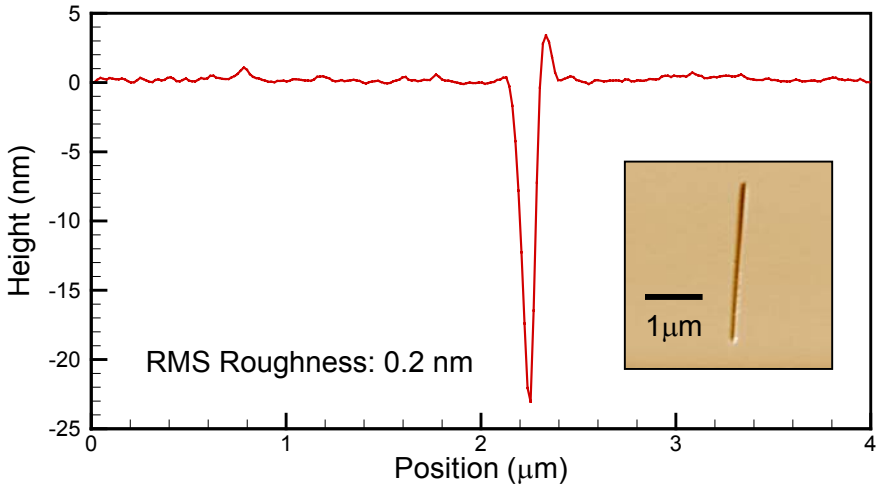

(a)

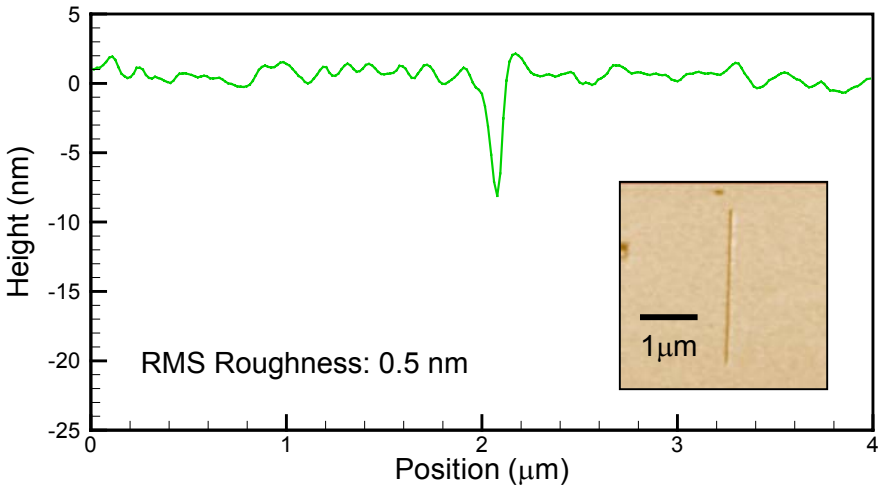

(b)

Figure 20. Profilometer characterization of as-deposited (top) and annealed (bottom) $AlMgB_{14}$ film on SiO_2 substrate. Note the improved scratch resistance (indicative of greater hardness) in the annealed film.

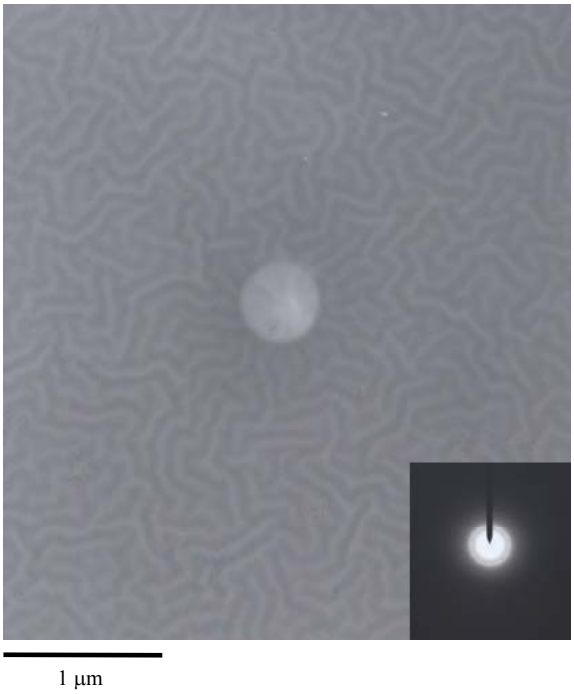

Figure 21. Bright field TEM image of the 573 K-deposited $AlMgB_{14}$ film (plan view). The inset shows the corresponding selected area diffraction pattern.

Given the promising results from the initial PLD trials, magnetron sputtering was subsequently investigated as an intermediate (and more cost effective) deposition technique for $AlMgB_{14}$. An industrial partner agreed to perform sputtering trials on 304 stainless steel substrates, using baseline boride targets hot pressed at Ames Laboratory. The Ames Laboratory machine shop constructed a special fixture to accommodate a hot pressed 1" diameter x 3/8" thick target. Because non-metallic targets such as the boride require relatively low operating pressures, precise control over the plasma column becomes difficult and premature termination of the plasma frequently occurs. Composition of the deposited films was determined at Ames Laboratory by XPS, and the results showed good agreement with the nominal composition of the target. Because of the relatively small size of the target, a small quantity of Fe, Cr, and Ni from the support ring was also sputtered into the films, which would have a deleterious effect on scratch resistance. Preliminary nanoindentation measurements indicate a hardness in the sputtered films at least that of the PLD films. Additional work is in progress to refine the deposition parameters to avoid contamination from the metal support structure.

Plans for Next Fiscal Year:

Work will continue on the synthesis and heat treatment of $AlCrB_{14}$ compounds. If successful, characterization of microhardness and fracture toughness will be performed on $AlMgB_{14}$, $AlCrB_{14}$, $AlCrB_{14}$ + TiB_2 (30% by weight), and $AlMg_{1-x}Cr_xB_{14}$ (where x = 0.1, 0.2, 0.3, 0.5, 0.75). In addition, low-speed, single point abrasion tests (scratch test) and high-speed, multi point abrasion tests (diamond abrasive belt test) will be performed. Multi-point abrasion tests will also be performed on $AlMgB_{14}$+Si planetary milled, $AlMgB_{14}$+Si spex milled, $AlMgB_{14}$+Si Zoz milled, SiC, WC+Co, $AlMgB_{14}$ + TiB_2 (30% by weight).

Analysis of high temperature diffusion tests on samples of baseline $AlMgB_{14}$ material with high-purity Ni, Co, and annealed Co-Mn (binder) will be performed. Results will be used to determine diffusion coefficients and activation energy for materials of industrial interest. The data will provide guidance in developing appropriate conditions for liquid-phase sintering of fully-dense cermet tools. In addition, the diffusion studies are necessary in order to establish the maximum service temperature of tools manufactured with these metal binders.

Production of material using the Zoz CM-01 for industrial evaluation will be continued. The powder produced from this device will be consolidated by inert gas pressing and by cold + hot isostatic pressing. A number of our industrial partners in the IMF program have requested kilogram quantities of material, which will require intensive processing activity. Thermal spray trials will require a portion of the material; in addition, material will also be made available to the University of Arkansas for expansion of their cutting test and tooling design efforts.

Evaluation of quasi-isostatic forging as a possible densification route for $AlMgB_{14}$ + binder cermets will be initiated. Isostatic forging is an established processing technology known to produce nearly fully dense ceramic + metal systems.

TEM characterization of pulsed laser deposited $AlMgB_{14}$ + TiB_2 films (on grids) will be performed; the objective is to determine if the goal of achieving a uniform, nanometric distribution of TiB_2 reinforcement phase was achieved. Since the nanohardness of baseline films (sans TiB_2) reached 50 GPa, it is anticipated that films containing the nanophase reinforcement will exhibit significantly higher hardness values, possibly extending further into the ultra-hardness range. Results will also have significant implications for processing of bulk $AlMgB_{14}$ + TiB_2 tool samples.

Patents

Provisional Utility Patent Serial No. 60/422,001, “Ductile Binder Phase for Use with $AlMgB_{14}$ and Other Hard Ceramic Materials "; B.A. Cook, A.M. Russell, and J.L. Harringa (ISURF #2949, filed October 29, 2002).

U.S. Patent 6,432,855, “Superabrasive Boride and a Method of Preparing the Same by Mechanical Alloying and Hot Pressing "; (divisional patent of 6,099,605) issued August 13, 2002, B.A. Cook, J. L. Harringa, and A.M. Russell.

U. S. Patent no. 6,099,605, “Superabrasive Boride and a Method of Preparing the Same by Mechanical Alloying and Hot Pressing,” issued August 8, 2000, B. A. Cook, A. M. Russell, and J. A. Harringa.

Provisional Patent Application filed: “An Ultra-hard, Low Friction Coating Based on $AlMgB_{14}$ for Reduced Wear of MEMS and other Tribological Components and Systems"; B.A. Cook, A.M. Russell, J.L. Harringa, P. Molian, A.P. Constant, and Y. Tian. (ISURF docket number 03035, AL490).

Intellectual Property Disclosure and Record, filed August, 2002, “ A New, Oxidation Resistant, Ultra-hard Material, Aluminum Chromium Boride, $AlCrB_{14}$"; B.A. Cook, A.M. Russell, and J.L. Harringa. (ISURF docket number 2951, AL484).

Intellectual Property Disclosure and Record, filed August, 2002, “ A New, Oxidation Resistant, Ultra-hard Material, Aluminum Titanium Boride, $AlTiB_{14}$"; B.A. Cook, A.M. Russell, and J.L. Harringa. (ISURF docket number 2950, AL483).

Intellectual Property Disclosure and Record, filed August, 2002, “Ductile Binder Phase for Use with $AlMgB_{14}$ and Other Hard Ceramic Materials "; B.A. Cook, A.M. Russell, and J.L. Harringa. (ISURF docket number 2949 (AT196)).

Publications/Presentations

Y. Tian, A. Bastawros, C.C. Lo, A. Constant, A.M. Russell, and B.A. Cook, "Superhard self-lubricating $AlMgB_{14}$ films for microelectromechanical devices,” Applied Physics Letters, 83 (2003) 1-3.

"Progress in Industrial Applications of a New Class of Ultra-Hard Borides", B.A. Cook, A.M. Russell, and D. Bhat, USDOE Office of Industrial Technology Conference on Industrial Materials of the Future, June, 2003, Golden, CO.

"Powder Metallurgical Processing of Ultra-hard Materials: Properties of Si-Ge, Al_2O_3, and $AlMgB_{14}$ Prepared by High-energy Zoz Milling", J.S. Peters, B.A. Cook, A.M. Russell, and J.L. Harringa, Powder Metallurgy and Particulate Materials Technology Conference (PM2TEC) sponsored by the Metal Powder Industries Federation, Las Vegas, NV, June, 2003.

"Powder Metallurgical Processing of Ultra-hard Materials: Properties of Si-Ge, Al_2O_3, and $AlMgB_{14}$ Prepared by High-energy Zoz Milling", Proceedings of the Powder Metallurgy and Particulate Materials Technology Conference (PM2TEC), submitted June, 2003 (in press).

B.A. Cook, A.M. Russell, J.L. Harringa, A.J. Slager, and M. Rohe, "A New Fracture-Resistant Binder Phase for Use with $AlMgB_{14}$ and Other Ultra-Hard Ceramics", Journal of Alloys and Compounds, accepted (in press).

Y. Tian, A. Constant, C.H.C. Lo, J.W. Anderegg, A.M. Russell, J.E. Snyder, and P. Molian, "Microstructure Evolution of Al-Mg-B Thin Films by Thermal Annealing", Journal of Vacuum Science and Technology A, Vol. 21, No. 4, pp. 1055-1063, 2003.

B.A. Cook, J. L. Harringa, T. L. Lewis, B. Lee, and A.M. Russell, "Processing Studies and Selected Properties of Ultra-hard $AlMgB_{14}$", Journal of Advanced Materials, (accepted, scheduled for publication in 2004).

J.M. Hill, D.C. Johnston, B.A. Cook, J.L. Harringa, and A.M. Russell, "Magnetization Study of the Ultra-hard Material $MgAlB_{14}$", Journal of Magnetism and Magnetic Materials, 265 (2003) 23-32..

T.L. Lewis, A.M. Russell, B.A. Cook, and J.L. Harringa, "Al_2MgO_4, Fe_3O_4, and FeB Impurities in $AlMgB_{14}$", Materials Science & Engineering A, Vol. 351, Issues 1-2, pp. 117-122, 2003.

B.A. Cook, J.L. Harringa, A.M. Russell, and S.A. Batzer, "A Proof-of-Concept Study of the Use of Complex Borides for Disassembly of Decommissioned Nuclear Reactor Containment Vessels", Machining Science and Technology, Vol. 7, No. 1, pp. 139-147, 2003.

A. Russell and B. Cook, "Crosscutting Industrial Applications of a New Class of Ultra-Hard Borides", IMF Newsletter: Industrial Materials for the Future, Winter, 2003, pp. 5-7.

R. Cherukuri, P. Molian, A. M. Russell, and Y. Tian, "A Feasibility Study of Pulsed Laser Deposited, New Superhard Tool Coatings for Metal Cutting," Surface Coatings and Technology, Vol. 155, pp. 112-120, 2002.

A.M. Russell, B.A. Cook, J. L. Harringa, and T. L. Lewis, "Coefficient of Thermal Expansion Determinations for $AlMgB_{14}$", Scripta Materialia, Vol. 46, pp. 629-633, 2002.

Y. Tian, M. Womack, P. Molian, C.C.H. Lo, J.W. Anderegg, and A.M. Russell, "Microstructure and Nanomechanical Properties of Al-Mg-B-Ti Films Synthesized by Pulsed Laser Deposition", Thin Solid Films, Vol. 418, pp. 129-135, 2002.

P. Molian and A. Russell, "A Feasibility Study of Pulsed Laser Deposited, New Superhard Tool Coating for Metal Cutting", at the 27th NSF Design, Service, and Manufacturing Grantees and *Research Conference, January, 2001, Tampa, FL.*

Milestone Status Table

ID Number	Task / Milestone Description	Planned Completion	Actual Completion	Comments
02-1	processing research			
02-1.1	mechanical alloying scale-up	1/1/03	03/31/03	Now implemented
02-1.2	composition development – I	9/30/02	9/30/02	(phase I)
02-1.3	cutting tests – I	9/30/02	12/15/02	(phase I)
02-1.4	microanalytical characterization - I	9/30/02	12/15/02	(phase I)
02-2	coating studies - I	ongoing		
02-3	tool design - I	ongoing		
03-1	processing research			
03-1.1	densification studies (binder phase)	9/30/03	9/30/03	HIP
03-1.2	composition development - II	9/30/03	9/30/03	
03-1.3	cutting tests - II	06/30/04	→→→→	In-progress
03-1.4	microanalytical characterization - II	3/31/04	→→→→	on-going support
03-2	coating studies - II	06/30/04	→→→→	In-progress
03-3	tool design - II	9/30/04	→→→→	In-progress
04-1	Processing/Densification research			
04-1.1	optimization of powder processing	12/31/03		
04-1.2	TiB_2 reinforcement phase	12/31/03		
04-1.2.1	Solution mixing	12/31/03		
04-1.4	quasi-isostatic forging	03/31/04		
04-2	Oxidation-resistant compositions			
04-2.1	Solubility limits of Cr in 1:1:14	01/31/04		
04-2.2	Two-phase composites	01/31/04		
04-3	Co-Mn Binder Phase			
04-3.1	Blending optimization	02/28/04		
04-3.2	Determination of best H_v & K_{1c}	03/31/04		
04-4	Tribology/surface studies			
04-4.1	complete scratch/abrasion tests	02/28/04		
04-4.2	mult-point abrasion tests	03/31/04		
04-4.3	determination of wear coefficient	04/30/04		

ID Number	Task / Milestone Description	Planned Completion	Actual Completion	Comments
04-5	Chemical reactivity			
04-5.1	diffusion coefficients	01/31/04		
04-5.2	activation energies	01/31/04		
04-7	Thin Film Coatings			
	Complete sputtering trials	12/31/03		
	Determine feasibility of HVOF	04/30/04		
04-8	Optimization of tooling design			
04-8.1	Completion of advanced cutting tests	04/30/04		
04-8.2	Development of performance models	05/31/04		
04-8.3	Prediction of tool life vs. parameters	06/30/04		
04-9	Commercialization (see footnote)[2]			
04-9.1	Draft business plan	10/31/03		
04-9.2	Preliminary market survey	2/28/04		
04-9.3	Final version of business plan	4/30/04		
04-9.4	Pilot-plant start-up	9/30/04		

[2] Viable Technologies, LLC, is the primary commercialization entity for this technology. Results of research described in this document are provided to Viable in support of its efforts.

Budget Data
(as of 09/30/03): (in thousands)

			Approved Spending Plan			Actual Spent to Date		
Phase / Budget Period			DOE Amount	Cost Share	Total	DOE Amount	Cost Share	Total
	From	To						
Year 1	10/01	09/30	$275	--	$275	$272(1)	--	$272(1)
Year 2	10/01	09/30	$255	--	$255	$255(2)	--	$255(2)
Year 3	10/01	09/30	$370	--	$370	$0		$0
Totals			$900	--	$900	$527	--	$527

(1) figure includes $55K to the University of Arkansas
(2) figure includes $35K to the University of Arkansas

Spending Plan for the Next Year

Month	Estimated Spending (thousands)	Comments
Oct. '03 (1)	$16	
Nov. '03 (1)	$16	
Dec. '03	$41	subcontractor pymt
Jan. '04	$17	
Feb. '04	$20	added HVOF research
Mar. '04	$20	
Apr. '04	$20	
May '04	$45	subcontractor pymt
Jun. '04	$20	
Jul. '04	$20	
Aug. '04	$20	
Sep. '04	$15	

As of 26 November, 2003, Congress had not passed the FY 2004 energy appropriation legislation. In the interim, laboratory operation are proceeding under continuing resolutions.